Direct Recognition of Superparamagnetic Nanocrystals by Macrophage Scavenger Receptor SR-AI

Ying Chao,[†] Priya P. Karmali,[‡] Rajesh Mukthavaram,[†] Santosh Kesari,[†] Valentina L. Kouznetsova,[§] Igor F. Tsigelny,[§,⊥] and Dmitri Simberg[∥,*]

[†]Neuro-Oncology Program, Moores UCSD Cancer Center, University of California San Diego, La Jolla, California 92093-0819, United States, [‡]Cancer Research Center, Sanford-Burnham Medical Research Institute, La Jolla, California 92037, United States, and [§]Department of Neurosciences, [⊥]San Diego Supercomputer Center, and [∥]Solid Tumor Therapeutics Program, Moores UCSD Cancer Center, University of California San Diego, La Jolla, California 92093-0819, United States

ABSTRACT Scavenger receptors (SRs) are molecular pattern recognition receptors that have been shown to mediate opsonin-independent uptake of therapeutic and imaging nanoparticles, underlying the importance of SRs in nanomedicine. Unlike pathogens, engineered nanomaterials offer great flexibility in control of surface properties, allowing addressing specific questions regarding the molecular mechanisms of nanoparticle recognition. Recently, we showed that SR-type AI/II mediates opsonin-independent internalization of dextran superparamagnetic iron oxide (SPIO) nanoparticles *via* positively charged extracellular collagen-like domain. To understand the mechanism of opsonin-independent SPIO recognition, we tested the binding and uptake of nanoparticles with different surface coatings by SR-AI. SPIO coated with 10 kDa dextran was efficiently recognized and taken up by SR-AI transfected cells and J774 macrophages, while SPIO with 20 kDa dextran coating or cross-linked dextran hydrogel avoided the binding and uptake. Nanoparticle negative charge density and zeta-potential did not correlate with SR-AI binding/uptake efficiency. Additional experiments and computer modeling revealed that recognition of the iron oxide crystalline core by the positively charged collagen-like domain of SR-AI is sterically hindered by surface polymer coating. Importantly, the modeling revealed a strong complementarity between the surface Fe—OH groups of the magnetite crystal and the charged lysines of the collagen-like domain of SR-AI, suggesting a specific recognition of SPIO crystalline surface. These data provide an insight into the molecular recognition of nanocrystals by innate immunity receptors and the mechanisms whereby polymer coatings promote immune evasion.

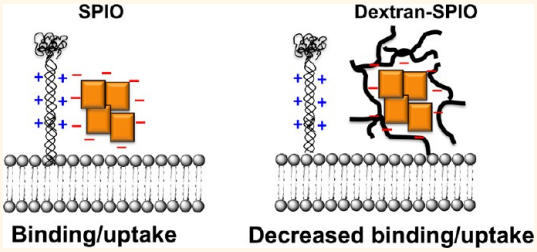

KEYWORDS: SPIO · CLIO · macrophage · scavenger receptor · dextran · hydrogel · charge

Nanomaterials interact in the body with a variety of extracellular plasma proteins,[1,2] as well as cell surface receptors on erythrocytes, platelets, leukocytes, and macrophages.[3] The complex interplay of these interactions is responsible for many phenomena observed for *in vivo* administered nanoparticles, including premature liver and spleen macrophage sequestration[4] and acute/chronic toxicity.[3] Two main innate immunity arms are actively involved in the body's first line of neutralization and clearance of foreign pathogens: (1) opsonin-independent mechanism (C-type lectins, scavenger receptors, Toll-like receptors) and (2) opsonin (plasma protein)-dependent mechanism (complement, IgM, fibronectin).[2,5,6] The same mechanisms appear to be relevant to the recognition of engineered nanoparticles and liposomes.[5,7] At the same time, the molecular basis of recognition of engineered nanomaterials by these defense systems is only partially understood. Scavenger receptors (SRs) are some of the most interesting and important phagocytic receptors that mediate *opsonin-independent* recognition and elimination of polyanionic molecular patterns, including apoptotic cells (*via* phosphatidylserine),[8,9] damaged proteins and lipoproteins,[10] lipopolysaccharides,[11] and viruses.[12] Several reports demonstrated that SRs mediate the uptake of engineered nanoparticles, including polystyrene,[13,14] quantum dots,[15] diesel particles,[16] DNA-gold,[17] titania, and maghemite nanoparticles.[16]

Superparamagnetic crystalline iron oxide (SPIO) is a significant magnetic resonance

* Address correspondence to dsimberg@ucsd.edu.

Received for review February 14, 2013 and accepted April 23, 2013.

Published online April 24, 2013
10.1021/nn400769e

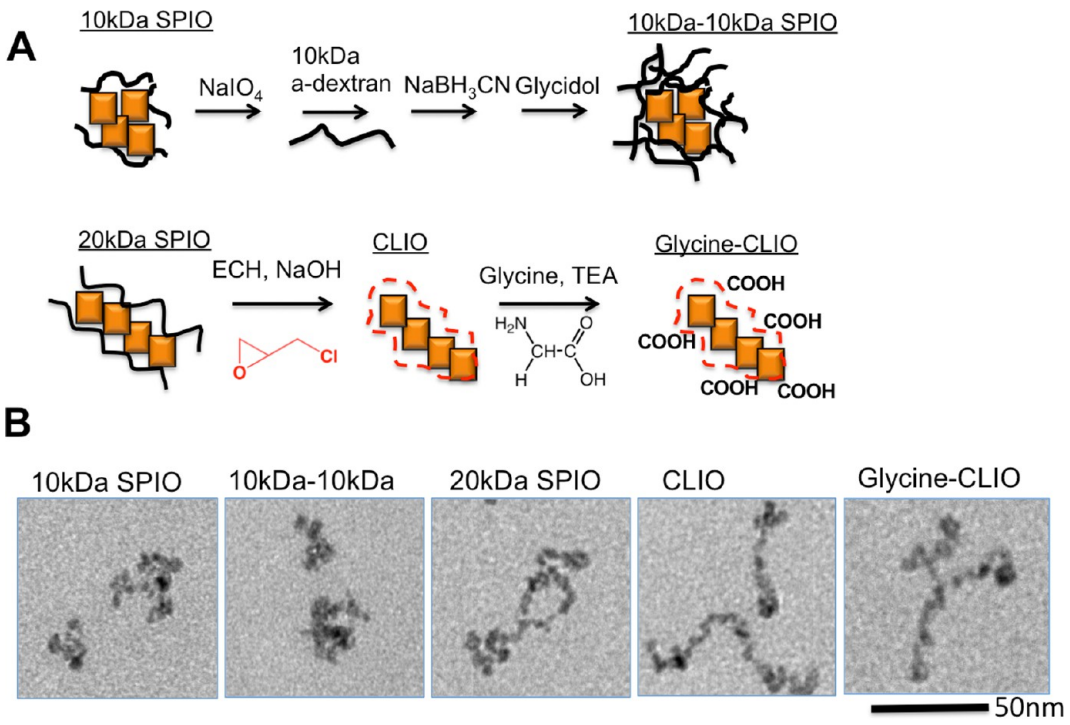

Figure 1. Preparation and modification of SPIO nanoparticles: (A) 10 kDa dextran-SPIO was modified with amino dextran by oxidation−Schiff base reduction method; 20 kDa dextran-SPIO particles were prepared from 20 kDa dextran by the precipitation method and cross-linked with epichlorohydrin in basic conditions. CLIO was further conjugated with glycine *via* residual epoxy groups (described in Methods). (B) Transmission electron microscopy images of various SPIO and CLIO without counterstaining (dextran and hydrogel are not visible). Size bar: 50 nm for all images.

imaging (MRI) contrast agent by itself and as a component of multifunctional nanomedicines for cancer imaging and treatment.[18−20] Dextran-SPIO consists of magnetite (Fe_3O_4)-maghemite (γ-Fe_2O_3) crystals of 5−10 nm size embedded in a meshwork of carbohydrate polymer dextran of 6−40 kDa molecular weight.[21] Recently, it has been reported that macrophage scavenger receptors, in particular, SR-AI/II,[22,23] play an important role in the uptake of dextran-SPIO by macrophages *in vitro*.[23−25] In addition, we recently demonstrated that SR-AI/II mediates recognition of 10 kDa dextran-SPIO (Feridex) *via* collagen-like domain (CLD) and suggested that the interaction is due to a very significant positive charge field on the CLD.[25] The surface of SPIO is always Fe^{3+} due to oxidation. The crystal surface is acidic[26−28] due to binding of water hydroxyls to Fe^{3+} and thus can interact with various organic bases.[29] However, it has been well-established[30−32] that being polyanionic is not the only requirement for scavenger receptor binding (*e.g.*, polyinosinic acid binds to SRs, while polyadenylic acid does not).

In view of these data, we sought to further understand the mechanisms of binding and uptake of SPIO nanocrystals by SR-AI. Since the surface coating and charge are some of the critical determinants of nanoparticle uptake by macrophages,[33−35] we were motivated to understand how SPIO coating and negative charge modulate the interaction with SR-AI. Numerous studies focused previously on the physicochemical properties that control nanoparticle binding and uptake by macrophages and monocytes,[4,33,34,36,37] but due to the intrinsic complexity of macrophage phagocytic machinery, it is difficult to address basic mechanisms of nanoparticle recognition. There is a significant interest in macrophage targeting for therapeutic and imaging applications, including magnetic cell labeling,[38] lipoprotein uptake blockade,[39] tumor macrophage imaging,[40] and immunotherapy.[41] On the opposite, there is a great interest in creating "stealth" nanomedicines that avoid the reticuloendothelial system for prolonged residence in blood.[4] Structure−activity studies in a simplified and more "clean" system of isolated phagocytic receptor in an opsonin-free environment can provide specific information on the molecular recognition of nanoparticles and may offer clues to the design of efficient nanoparticulate systems.

RESULTS AND DISCUSSION

To study the effect of surface coating on the direct recognition of SPIO by SRs, we prepared SPIO with the following surface coatings (Figure 1A and Methods): (a) 10 kDa dextran-coated SPIO (hereafter 10 kDa SPIO) was either obtained commercially (Feridex) or synthesized by precipitation of Fe^{2+} and Fe^{3+} in the presence 10 kDa dextran; (b) 10 kDa dextran was conjugated to the 10 kDa SPIO coating of by oxidation−Schiff base reduction method to produce 10 kDa-10 kDa SPIO; (c) 20 kDa SPIO was synthesized by precipitation method

TABLE 1. Size and Zeta-Potentials of SPIO Formulations with Different Surface Coatings

particle	*Z*-average diameter (PDI)	zeta-potential, mV
10 kDa SPIO	85 nm (0.24)	−13.1
CLIO	82 nm (0.15)	−5
10 kDa-10 kDa SPIO	101 nm (0.25)	−5.5
20 kDa SPIO	92 nm (0.20)	−7.3
glycine-CLIO	75 nm (0.12)	−15
20 kDa dextran	NM	−1.1

using 20 kDa branched dextran; (d) cross-linked hydrogel CLIO[2,42] was prepared by reacting 20 kDa SPIO with epichlorohydrin in basic conditions; (e) CLIO was further reacted with glycine (*via* residual epoxy groups) to increase the negative charge of the hydrogel shell. Epoxide chemistry is routinely used to conjugate ligands *via* amino groups to the CLIO hydrogel surface.[43] All of the particles had average hydrodynamic diameters between 75 and 101 nm (Table 1). Dextran-iron oxides prepared by precipitation possess broad size distribution;[44] our formulations had polydispersity indexes (PDI) between 0.12 (glycine-CLIO) to 0.25 (10 kDa-10 kDa SPIO). Since dextran-SPIO particles are not ideally spherical, the contribution of dextran thickness to the nanoparticle size is not straightforward from DLS measurements. All formulations were negatively charged: 10 kDa SPIO had zeta-potential of −13 mV, while increasing the size of dextran or cross-linking the dextran resulted in a decrease of negative zeta-potential (Table 1). Addition of glycine to CLIO resulted in negative zeta-potential of −15 mV. Dextran 20 kDa was neutral (Table 1), suggesting that the negative charge of SPIO originates from the crystalline iron oxide core, which is supported by the literature.[26] According to transmission electron microscopy (TEM) images (Figure 1 and Supporting Information Figure S1), the particles appeared as clusters of 5−10 nm crystals. The shape of 10 kDa SPIO and 10 kDa-10 kDa SPIO was mostly irregularly spherical, whereas the shape of 20 kDa SPIO, CLIO, and glycine-CLIO was elongated "worm-like" (we term them magnetic nanoworms[2,43]).

Dextran and Cross-Linked Dextran Block Scavenger Receptor-Mediated Uptake. Scavenger receptors play an important role in the opsonin-independent uptake of 10 kDa SPIO. Western blotting (Supporting Information Figure 2) showed the enrichment of SR-AI/II on 10 kDa SPIO when incubated with J774.A1 monocyte−macrophage cell line lysate (see Supporting Information). To test the role of surface dextran in the uptake by J774.A1 macrophages in opsonin-free, nanoparticles with different surface coatings were added to the cells in 10% FBS-supplemented DMEM for 2 h (optimal time point determined in our previous studies).[25] DLS analysis showed no significant aggregation of 10 kDa SPIO, 20 kDa SPIO, and CLIO formulations in cell medium (Supporting Information Figure 3). According to Prussian blue staining (Supporting Information Figure 4) and iron assay quantification (Figure 2A), 10 kDa SPIO showed efficient accumulation in J774A.1 macrophages. Polyinosinic acid, a well-known polyanionic inhibitor of SR uptake,[10] reduced the binding and uptake (Figure 2A and Supporting Information Figure 4) of 10 kDa SPIO by 81% ($P = 0.0026$, *t* test, $n = 5$), confirming that 10 kDa SPIO uptake by J774A/1 macrophages is mediated *via* scavenger receptor mechanism. According to Figure 2A and Supporting Information Figure 4, the binding and uptake of 10kDA-10 kDa SPIO, 20 kDa SPIO, and CLIO was 70−77% less ($P = 0.0037$, *t* test, $n = 5$) that 10 kDa SPIO.

After establishing the dominant role of SRs in opsonin-independent recognition of SPIO by macrophages, in the subsequent experiments, we focused on molecular mechanisms of recognition of nanoparticles as well as the role of surface coating in the binding and uptake by S-AI in a simplified and well-characterized system of transiently transfected nonphagocytic cells.[25] SR-AI and SR-AII are the splicing isoforms of the same receptor; both possess an identical CLD that mediates recognition of anionic ligands[30] and SPIO.[25] Both receptor isoforms have been previously shown by us to efficiently bind and internalize 10 kDa SPIO (Feridex).[25] Nanoparticles with different surface coatings were incubated with HEK293T cells transfected with SR-AI in FBS-supplemented DMEM. According to Figure 2B,C and Supporting Information Figure 5, there was a significant binding and uptake of 10 kDa SPIO by SR-AI-transfected cells but not by vector (pcDNA3)-transfected cells. According to Figure 2B,C and Supporting Information Figure 5, the binding and uptake of 20 kDa SPIO, CLIO, and 10 kDa-10 kDa SPIO was 83, 87, and 78%, respectively, lower than that of 10 kDa SPIO (*p*-value 0.0065, *t* test, $n = 5$ for 20 kDa SPIO), suggesting similar effect of surface coating on macrophages and SR-AI-transfected cells.

To confirm that surface coating prevents the binding of nanoparticles to SR-AI, we immobilized recombinant His-tagged SR-AI on Ni^{2+}-NTA agarose beads and incubated them with 10 kDa SPIO, CLIO, and 20 kDa SPIO in PBS. According to Figure 2D,E, 20 kDa SPIO and CLIO showed 80 and 83%, respectively, less binding that 10 kDa SPIO (*p*-value <0.0001, *t* test, $n = 5$). When 20 kDa SPIO was treated with Dextranase (1,6-α-D-glucan-6-glucanohydrolase), a bacterial enzyme that cleaves α-1,6 linkages of dextran,[45] this treatment restored the binding of SPIO to the SR-AI beads (Figure 2D,E). Unfortunately, since the particles aggregated in cell medium after the digestion of surface coating, we were not able to test the role of Dextranase on SR-AI binding and SR-AI uptake in cell medium. CLIO and 20 kDa SPIO have a worm-like shape, while 10 kDa SPIO has an irregular "spherical" shape (Figure 1A and Supporting Information Figure 1). Particle shape is an important factor in nanoparticle uptake, and elongated nanoparticles have been shown

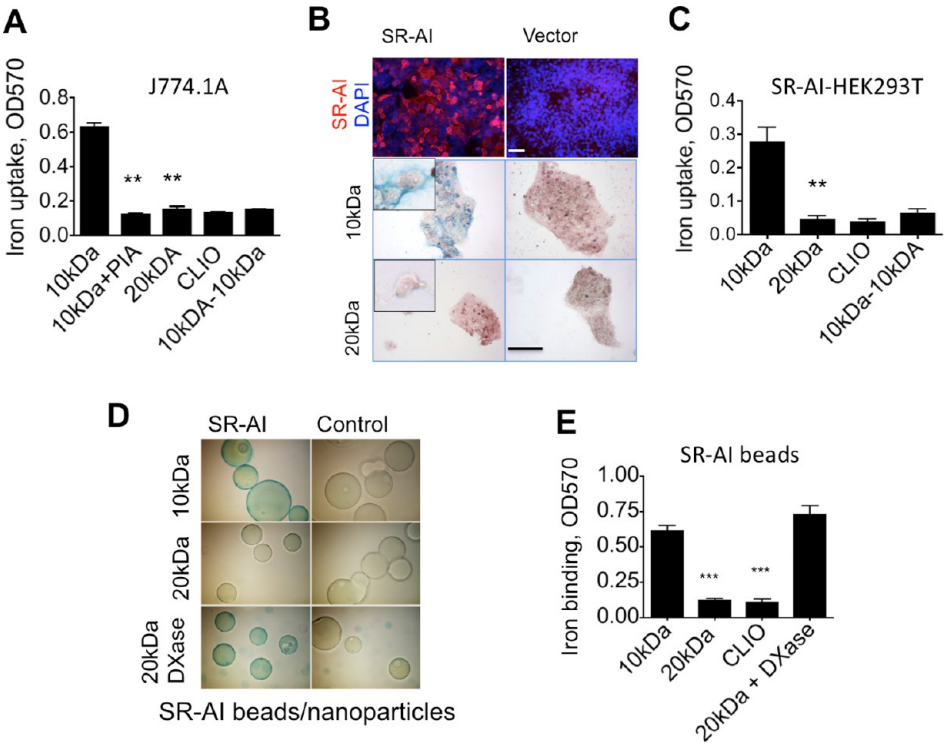

Figure 2. The 20 kDa dextran and hydrogel coating block the binding and uptake *via* SR-AI. (A) Binding and uptake by J774.A1 macrophages following incubation with nanoparticles at 0.1 mg/mL was quantified with iron assay. Dextran 20 kDa and hydrogel coating and polyinosinic acid (PIA) block the binding and uptake (nonpaired *t* test, $n = 5$). (B) Top row: HEK293T cells were transfected with SR-AI-coding plasmid using Lipofectamine 2000, and the receptor expression was visualized with anti-SR-AI/II antibody (red). Transfection efficiency was over 70%. Size bar 50 μm. Middle and bottom: transfected cells were incubated with nanoparticles at 0.1 mg/mL. The binding and uptake of iron was visualized with Prussian blue (blue stain), and the nuclei were counterstained with nuclear fast red (red stain). The 10 kDa SPIO shows the highest binding and uptake, whereas 20 kDa SPIO does not show any visible staining. Insets show individual cropped cells (from another field) demonstrating binding and internalization of 10 kDa SPIO and no visible binding and uptake of 20 kDa SPIO. No significant binding and uptake by control plasmid-transfected cells (pcDNA3.1) was observed under these conditions. Note that HEK293T cells grow in clusters, and the cell density is higher in the top row of images. Size bar is 200 μm for middle and lower rows. (C) Quantification of iron uptake by SR-AI-transfected cells shows a significant decrease in the binding and uptake of dextranated and hydrogelated SPIO (nonpaired *t* test, $n = 5$). (D) Binding of SPIO to agarose beads coated with recombinant SR-AI (see Methods) as a function of dextran coating. The 10 kDa SPIO show efficient binding to the beads as detected with Prussian blue stain (green-blue color). The 20 kDa dextran coat blocks the binding to the beads, while the digestion of dextran with Dextranase (DXase) restores the binding. No binding to control beads (noncoated beads) was observed (right column). (E) Quantification of iron binding to the SR-AI beads with iron assay (nonpaired *t* test, $n = 5$).

to exhibit lower cell uptake for gold and polystyrene nanoparticles.[46−48] However, 10 kDa-10 kDa SPIO, which has the irregular spherical shape, showed 78% less uptake by SR-AI-transfected cells than the parent 10 kDa SPIO particles (Figure 2C), and digestion of dextran on worm-like 20 kDa SPIO promoted the binding to SR-AI (Figure 2D). Therefore, we conclude that surface coating rather than shape is the major determinant of binding efficiency of SPIO by SR-AI and, consequently, the uptake efficiency by SR-AI-transfected cells.

SR-AI-Mediated Uptake Does Not Correlate with the Nanoparticle Negative Charge. Negative zeta-potentials of 20 kDa SPIO, 10 kDa-10 kDa SPIO, and CLIO were somewhat decreased compared to 10 kDa SPIO (Table 1), possibly as a result of a shift in shear plane farther from the crystalline surface. To test whether dextranation and hydrogelation mask the negatively charged crystalline core, we tested the binding of protamine sulfate, a small cationic arginine-rich protein (5 kDa), to 10 kDa SPIO, 20 kDa SPIO, and CLIO. The binding of protamine sulfate turned the zeta-potential of all of the particles from negative to positive (+9.3 mV for 10 kDa SPIO, +9.4 mV for 20 kDa SPIO, and −8.3 mV for CLIO). SDS-PAGE analysis showed that 10 kDa SPIO, 20 kDa SPIO, and CLIO absorbed protamine sulfate to the same extent (Figure 3A). We also compared the binding of high molecular weight kininogen, a 120 kDa plasma protein, which absorbs to SPIO through histidine-rich domain D5.[49] The particles were mixed with mouse plasma, washed, and the protein was detected with Western blotting. Similarly to protamine sulfate, the same level of binding to all SPIO formulations was observed (Figure 3B). These data suggest that the crystalline core charges are not neutralized by dextran and hydrogel coating and are available for interactions with globular cationic proteins.

To test if negative charge determines the binding and uptake by SR-AI, we added negative charges to the

hydrogel coat of CLIO by conjugating glycine to residual epoxy groups (Figure 1). We chose this strategy because cross-linked hydrogel is stable and allows more extensive modifications than non-cross-linked dextran. Following the conjugation, zeta-potential increased from −5 mV to −15 mV (Table 1 and Figure 4A). Despite the fact that glycine CLIO had the same zeta-potential as 10 kDa SPIO, these particles showed only about 20% uptake by SR-AI-transfected cells (Figure 4B, *p*-value 0.0022, *t* test, $n = 5$).

The experiments above suggest that the charge *per se* does not determine the efficiency of uptake by SR-AI. To test this hypothesis for other nanoparticle types, we prepared large unilamellar liposomes with different mole ratios of negatively charged lipid dipalmitoyl phosphatidylserine. Phosphatidylserine is a natural ligand of scavenger receptors.[8,9] The liposomes were extruded through a 0.1 um membrane to yield sizes between 140 and 200 nm (Supporting Information Figure 6) and zeta-potential between −65 and −85 mV (Figure 4C). DPPS 100% liposomes were efficiently taken up by SR-AI-transfected HEL293T cells (Figure 4D and bound to SR-AI beads (Figure 5E). However, the uptake of DPPS/DPPC (2:1) drastically decreased by 74%, while the uptake of DPPS/DPPC (1:1) was almost nondetectable (Figure 4D). Also, DPPS/DPPC (1:1) did not bind to SR-AI coated beads (Figure 4E). Control beads and nontransfected cells did not show much binding and uptake (Supporting Information Figure 7). The negative surface charge density of DPPS 100% is approximately 1/nm^2, while that of

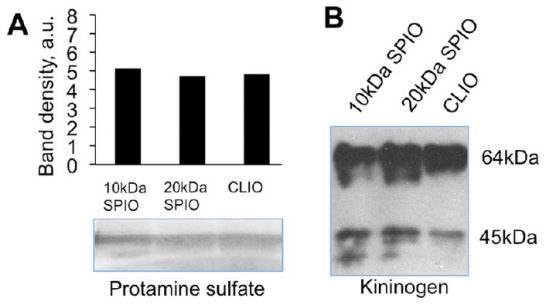

Figure 3. The 20 kDa dextran and hydrogel coating do not inhibit binding of cationic proteins to SPIO. SPIO with different surface coatings was tested for binding of salmon sperm protamine sulfate or mouse plasma kininogen as described in Methods. (A) Protamine sulfate bound to the particles. The bands were quantified using ImageJ program. There was no difference in the binding to all formulations. (B) Binding of plasma kininogen was detected with Western blotting. Similar to protamine sulfate, there was no difference in the binding to 10 kDa SPIO, 20 kDa SPIO, and CLIO. The bands show kallikrein-mediated cleavage of single-chain high molecular weight kininogen (120 kDa) into heavy and light chains.

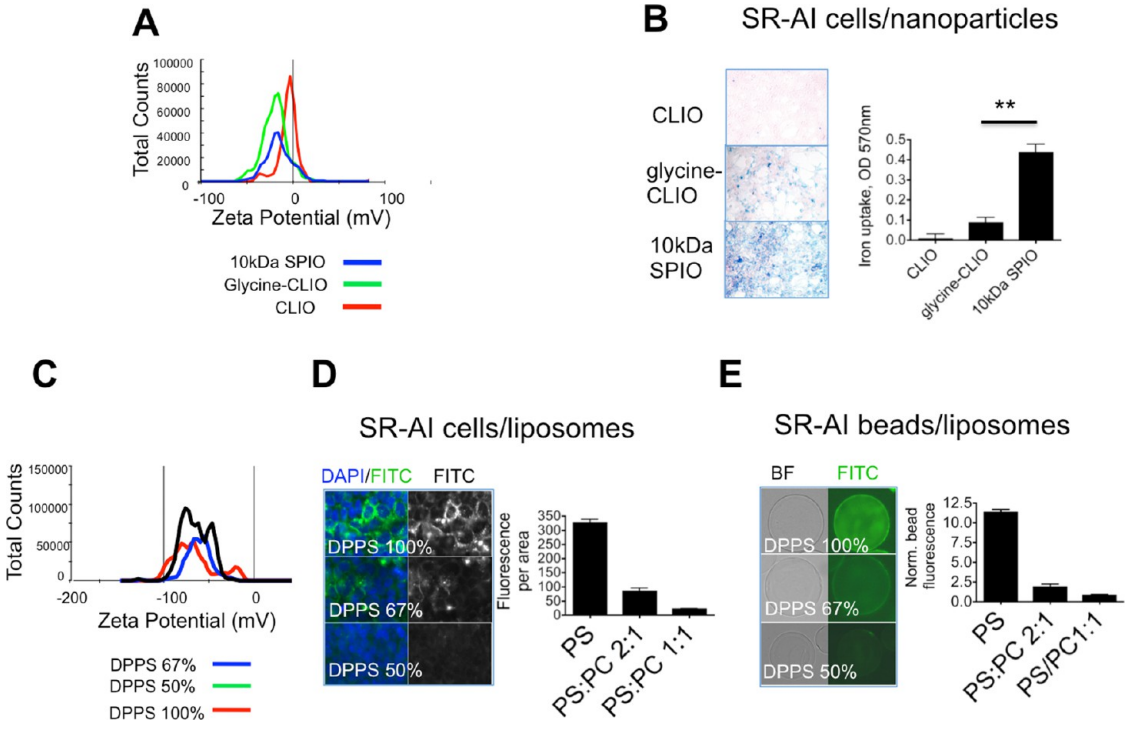

Figure 4. Anionic charge (zeta-potential) does not correlate with SR-AI uptake. (A) CLIO was reacted with glycine in basic conditions to increase the negative charge on the particles as described in Methods. Following incubation at 0.2 mg/mL for 2 h, the uptake by SR-AI-expressing cells was visualized with Prussian blue staining. (B) Quantification of uptake shows that, despite the same zeta-potential as 10 kDa SPIO, glycinated CLIO shows only about 20% of the uptake (nonpaired *t* test, $n = 5$). (C) Pure DPPS or mixed DPPS/DPPC liposomes were prepared by dehydration−rehydration−vortexing−extrusion. Liposomes were fluorescently labeled with 0.3 mol % of fluorescein-dioleyl phosphatidylethanolamine. (D) Liposomes were added to the SR-AI-transfected 293T cells, and total lipid and fluorescent lipid concentration (0.5 mM) were constant for all formulations. At 67% DPPS, there is a marked decrease in the SR-AI binding and uptake, while 50% DPPS liposomes do not show visible binding and uptake. (E) Binding to SR-AI-coated beads (Methods) shows excellent correlation with cell uptake studies described above.

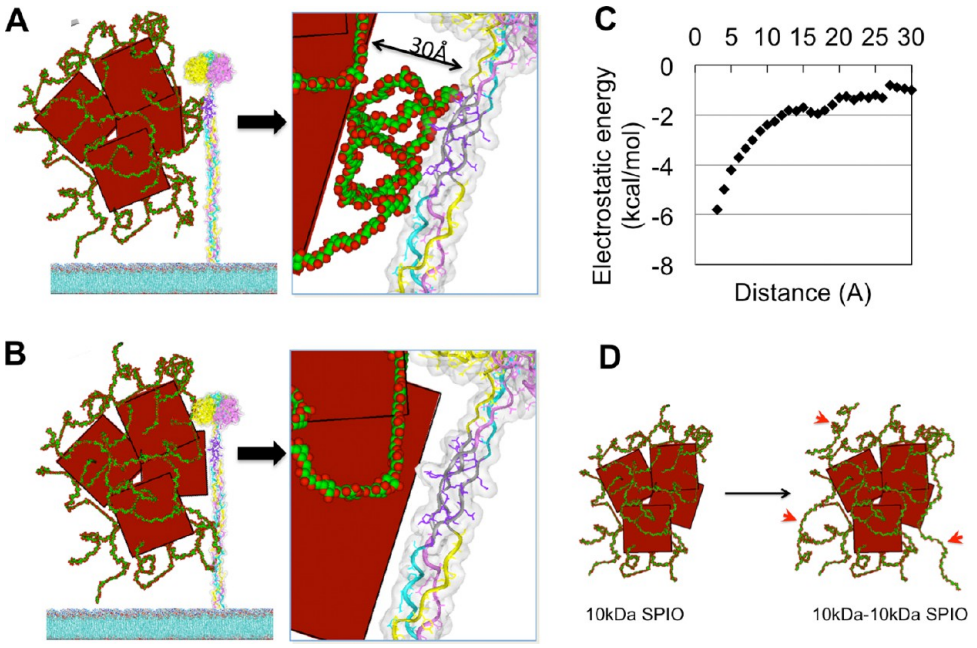

Figure 5. Modeling of SR-AI-SPIO binding. The receptor and nanoparticle were modeled as described in Methods. Modeling shows real size relationship between the SR-AI extracellular part and 10 kDa dextran-SPIO. (A) SPIO interacts with the charged collagen-like domain (CLD), while dextran is sandwiched between. (B) SPIO interacts with SR-AI CLD in the areas incompletely covered by dextran chains. (C) Calculation of electrostatic attraction energy between SR-AI positive charge field[25] and the crystal face anionic charge (4 per 100 nm^2). The interaction is not feasible at distances comparable to the thickness of dextran layer (30 Å), suggesting that the receptor binds to SPIO in areas not coated by dextran. (D) Conjugation of 10 kDa dextran (red arrows) to 10 kDa SPIO leads to the masking of the "naked" crystal surface, making it impossible for the receptor to bind. Note that dextran chains are of different lengths because this is a 2-D projection of 3-D conformations.

DPPS 50% is approximately 0.5/nm^2 (assuming that each serine headgroup has the cross-sectional area of approximately 0.5 nm^2 and a charge of −1 at physiological pH).[50] Based on titration studies,[29,51] negative surface charge density of both magnetite and maghemite at neutral pH 7.4 is less than 10×10^{-3} coulomb/m^2, or <0.059 electron/nm^2. At pH >12, when all proton donors are ionized, the negative charge density would be 0.99/nm^2.[51] Surface charge density of comparable 100 nm diameter polystyrene particles with zeta-potential of −10 mV was previously calculated at 6.8×10^{-3} coulomb/m^2, or 0.04 electron charges per nm^2.[52] Based on this evidence, we assumed surface charge density of magnetite-maghemite crystals at 0.04/nm^2. Therefore, a DPPS 50% liposome has about 10 times higher charge density than a SPIO crystal. Since DPPS 50% liposomes did not show appreciable binding and uptake, as opposed to efficient binding and uptake of 10 kDa SPIO, it is reasonable to suggest that SR-AI binding and uptake is mediated *via* specific recognition mechanisms rather than plain electrostatic attraction.

Computer Simulation of Interaction between SR-AI and SPIO. The experiments above suggest that SR-AI recognizes the Fe_3O_4 crystalline core while surface coating blocks the binding. To get a better insight into molecular mechanisms of recognition of SPIO as well as the mechanisms by which surface coating interferes with the binding, we used our previously described charge model of SR-AI.[25] SPIO was modeled as a cluster of 10 nm crystals covered with 10 kDa dextran chains (Figure 5A). This model is consistent with the looplike absorption of polymer chains onto the maghemite surface (the fully stretched 10 kDa dextran molecule charge is around 40−50 nm)[53] with approximately 2−3 dextran molecules absorbed per crystal.[28]

We hypothesize that two modes of interaction are possible: (a) direct binding of SR-AI collagen-like domain (CLD) to the crystalline surface (Figure 5A); (b) electrostatic attraction between CLD and the anionic crystal with dextran chains sandwiched between (Figure 5B). The latter scenario is possible only if the attraction force is sufficiently strong. We calculated the electrostatic energy of interaction between CLD positive charge field that we modeled previously[25] and one face of the 10 nm crystal (4 negative charges per 100 nm^2). According to Figure 5C, the electrostatic energy drops sharply at 15 Å from the crystalline surface (from −5.8 kcal/mol at 3 Å to −1.7 kcal/mol at 15 Å) and reaches background plateau at 20−30 Å. Studies by Jung[28] and others[27,44] showed that 10 kDa dextran adds between 33 and 100 Å to the surface thickness, which is consistent with our model (Figure 5B). Based on these data, CLD can interact with the particle only in the areas not covered or minimally covered with dextran. The model shows that there are multiple "gaps" in the dextran coat, and incomplete coverage of SPIO surface by 10 kDa dextran was

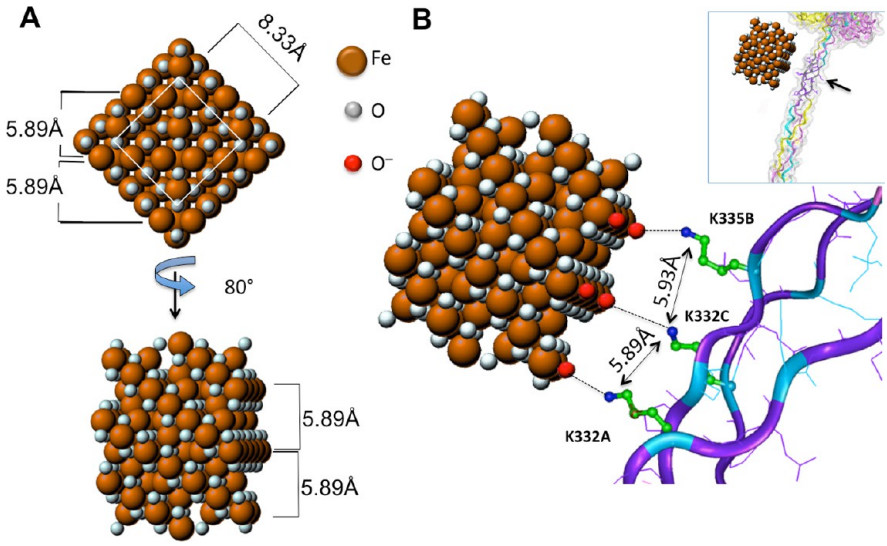

Figure 6. Proposed model of interaction between the charged lysine cluster in SR-AI and the crystalline magnetite (one unit cell). (A) Two-dimensional frontal and rotated projections of the magnetite unit cell. Albeit SPIO surface is maghemite due to oxidation, the spinel structure and unit cell dimensions are almost identical. White square shows the dimensions of the maghemite unit cell (8.33 Å). Therefore, surface planes of the Fe^{3+} cations have periodicity of 5.89 Å. (B) Three-dimensional view of the crystal unit approaching the charged domain in CLD. The crystal was scaled to real receptor dimensions. Oxygen of Fe−OH is shown in red (not all surface Fe^{3+} are hydroxylated).[26] The distance between spatially arranged lysines on the receptor's collagen triplex nicely match the periodicity of the surface Fe−OH planes. Lysine side chains' atoms are not scaled to the crystal's atoms. One lysine cluster out of three is shown.

previously demonstrated.[28] For 10 kDa-10 kDa SPIO, additional 10 kDa chains (Figure 5D, red arrows) should further hinder the access to the crystal surface. It is remarkable that the dextran coating still leaves relatively large pores and defects that can allow access of smaller, more flexible proteins including protamine sulfate and kininogen. It was previously demonstrated that stealth coatings (PEG, dextran, Poloxamer, hydrogel) do not efficiently prevent binding of plasma proteins to nanoparticles,[2,54,55] and our model of surface coating can explain this phenomenon.

In our experiments, negatively charged DPPS 50% liposomes and glycine-CLIO were not efficiently recognized by SR-AI. Both SR-AI and SR-AII recognize polyanionic ligands *via* a charged lysine cluster in the highly conserved motif GPKGQKGEK.[30,56] Previous work using polyanionic polymers and lipoproteins suggested that efficient ligand recognition by SR-AI/II requires correct spacing and alignment between the receptor's lysines and the ligand's anionic groups.[30,57] Therefore, we questioned whether there is a complementarity between the SPIO crystal and SR-AI charged domain. The spinel structure of magnetite and magnetite has a high level of planar order (Figure 6A). Magnetite and maghemite have similar unit cell dimensions (lattice parameter a = 8.397 and 8.33 Å, respectively).[58] Since the surface of SPIO magnetite crystal is maghemite due to air oxidation,[28] we used maghemite dimensions to calculate interplanar distance between the surface Fe^{3+} planes at 5.89 Å (Figure 6A). The alignment of the magnetite unit cell with the charged collagen triplex showed a striking complementarity between the acidic Fe−OH planes and the spatially arranged lysine side chains K332A, K332C, and K335B (Figure 6B). It is likely that this type of complementarity does not exist for highly anionic but otherwise less ordered surfaces of DPPS 50% and glycine-CLIO particles. It is also obvious that sterical interference by surface polymer coating could severely disturb the delicate alignment of charges and lead to a complete loss of binding, something that we observed in our experiments.

CONCLUSIONS

The results unambiguously show that increasing molecular weight of SPIO dextran coating, or forming a cross-linked hydrogel coat, leads to a complete loss of SR-AI binding and uptake. Collectively, the data suggest that SR-AI recognizes the charged crystalline core of iron oxide nanoparticles, while polymer coating sterically prevents the interaction. Computer modeling demonstrates that the binding of collagen-like domain of SR-AI to Fe_3O_4 crystalline core takes place in the areas without polymer coverage. Furthermore, the fact that magnitude of anionic charge does not correlate with SR-AI recognition brings up a hypothesis of a specific recognition mechanism of the crystalline lattice's charges. Such mechanism could also be relevant for titania and silica particles that are avidly recognizable by scavenger receptors.[16] Albeit *in vivo* recognition mechanisms are inherently more complex[5,59] and possibly involve plasma protein corona and complement,[6,7] our *in vitro* data are an important advance in understanding the phenomenon of nanoparticle immune

recognition by macrophage receptors and could bear important implications on the design of nanoparticulates for variety of therapeutic and imaging applications. For example, the knowledge of how iron oxides are recognized by immune receptors could be used for more efficient "camouflaging" of the nanoparticle surface. As a consequence, the increased circulation time can allow reducing the injected dose and achieving better tumor accumulation and MR imaging contrast. Another important application of the structure-recognition rules described herein could be in a more specific targeting to scavenger receptors for antibacterial and antiatherosclerosis therapies.[39,60] Future studies will focus on the interplay between scavenger receptors and plasma factors (complement) in the recognition of SPIO by macrophages *in vivo*.

METHODS

Nanoparticle Synthesis and Characterization. SPIO coated with 10 kDa or 20 kDa dextran (hereafter 10 kDa SPIO and 20 kDa SPIO) was prepared by precipitation of Fe^{2+} and Fe^{3+} salts in ammonia in the presence of branched dextran, as described elsewhere in the literature.[28,44,61] Feridex intravenous (i.v.) nanoparticles coated with 10 kDa (T-10) dextran were obtained from the UC San Diego Department of Radiology. Particles were resuspended in phosphate buffered saline (PBS) at 1−2 mg (Fe)/mL and filtered through a 0.2 μm membrane filter. For conjugation of 10 kDa dextran molecules to the existing 10 kDa dextran coat of Feridex, 0.1 mg of sodium periodate (Sigma-Aldrich, St. Louis, MO) was added to 1 mL of nanoparticles at 2 mg/mL Fe. After stirring at 4 °C overnight, the particles were extensively dialyzed against PBS and added to the excess amount (1 mg Fe/20 mg dextran) of aminated 10 kDa dextran (Life Technologies, Carlsbad, CA). After 24 h mixing at 4 °C, the particles were washed three times with ultracentrifugation at 70 000*g* for 10 min using a Beckman-Coulter TLA-100 ultracentrifuge (Brea, CA), then reduced with 10 mg/mL sodium cyanoborohydride (Sigma-Aldrich) for 5 h at room temperature and dialyzed against double-distilled water (DDW) overnight. The residual primary amines were blocked by incubation with 0.5% v/v glycidol (Sigma-Aldrich) for 4 h at room temperature. The washed particles were stored in PBS at 4 °C prior to use. Cross-linking of 20 kDa SPIO with epichlorohydrin was performed according to a previously described protocol with modifications.[25] Briefly, 2 mg/mL (iron) solution was mixed with one part of 5 N NaOH 1:1 and one part of epichlorohydrin (Sigma-Aldrich) and incubated overnight. The particles were dialyzed in DDW overnight. To conjugate glycine groups, the CLIO solution in DDW was incubated with 5 mg/mL solution of glycine and 1% triethanolamine (both from Sigma-Aldrich) overnight. The particles were washed by ultracentrifugation as described above.

Nanoparticle and liposome size (intensity distribution) was measured using a Zetasizer Nano (Malvern Instruments, Worchestershire, UK) by diluting 20−30 μL of 1 mg/mL particle solution in 1 mL DDW. Zeta-potential (ζ) was measured with the same instrument at the same particle solution in 1 mL of DDW. This volume of PBS was just sufficient to keep the pH at neutral (pH 7.23) without damaging the electrodes of the zeta cell. For nanoparticle imaging with transmission electron microscopy, the nanoparticle solution in water was placed on Formvar/carbon-coated grids (Ted Pella, Redding, CA). After 5 min, the grid was gently blotted and air-dried. All samples were studied without counterstaining. Grids were viewed using a JEOL 1200EX II transmission electron microscope at 75 kV and different instrumental magnifications. Images were captured using a Gatan digital camera.

Plasmid Preparation and Receptor Transient Expression. Full-length mouse cDNA of SR-AI (splicing variant A, NM_001113326) was amplified from mouse liver mRNA by reverse transcription PCR using the following primers: forward, GCAGTC GGATCCATGACAAAAGAGATGACAGAGAATC, reverse, GCAGTCCTCGAGTTATGAAGTACAAGTGACCCCAG. The amplified CDNA was subsequently cloned into pCDNA 3.1+ Zeo plasmid (Life Technologies) using the *Bam*HI and XhoI restriction sites. Human embryonic kidney cells HEK293T were maintained in Dulbecco's modified Eagle medium (DMEM)/high glucose media (Thermo Scientific HyClone, Logan, UT) supplemented with 10% fetal bovine serum and 1% penicillin-streptomycin-L-glutamine solution).

For transfection experiments, cells were seeded at a density of 0.5−1 × 10^6 cells/well in 24-well plates and transiently transfected with 0.5 μg of receptor plasmids or empty vector pCDNA 3.1 using Lipofectamine 2000 (Life Technologies) as per the manufacturer's instructions. The expression of SR-AI/II on the cell surface was tested by immunostaining with rat anti-mouse SR-A antibody which detects both SR-AI and SR-AII isoforms (R&D Systems, Minneapolis, MN). The same antibody was used for Western blotting of the receptor.

Nanoparticle Uptake Experiments. Mouse monocyte cells J774a.1 and monkey kidney HEK293T cells were obtained from the American Tissue Culture Collection (ATCC) and maintained in DMEM supplemented with 10% heat-inactivated fetal bovine serum, L-glutamine, and antibiotics. Nanoparticle uptake quantification in receptor-transfected cells and J774A.1 cells was performed as described elsewhere.[59] Briefly, the cells were incubated with 0.1−0.2 mg/mL (Fe concentration) for 1−2 h in complete medium at 37 °C. At the end of the incubation, the cells were washed two times with serum-free DMEM followed once with PBS, and iron uptake was quantified using Quanti-Chrom iron assay (BioAssay Systems, Hayward, CA). For the uptake visualization, the experiment was performed in 8-well chamber slides (NalgeNunc, Rochester, NY). Following incubation with 0.1 mg/mL iron for 2 h, the cells were washed three times as described above, fixed with 4% formaldehyde, and stained with Prussian blue dye.[62] Nuclei were counterstained with nuclear fast red. For the ligand inhibition, polyinosinic acid (Sigma-Aldrich) at 50 μg/mL was incubated with cells for 15 min prior to the addition of nanoparticles.

Binding of Cationic Proteins to Nanoparticles. SPIO was incubated at various weight ratios with salmon sperm protamine (Sigma-Aldrich) in PBS for 10 min at room temperature. The unbound protein was washed away four times using a Beckman-Coulter TLA-100 ultracentrifuge (70 000*g* for 10 min in 1 mL of PBS) to make sure there was no free protamine sulfate, and the pellet was boiled in 50 μL of 8 M urea/1 M NaCl/1 M imidazole for 30 min. The mixture of particles and proteins (corresponding to 5 μg iron) was subsequently loaded into wells of Novex 4−20% Tris-glycine polyacrylamide gel (Life Technologies), and the proteins were electrophoretically separated and stained with a SilverQuest kit (Life Technologies). The protamine was located at around 6 kDa M_w.

Kininogen binding experiments were performed by mixing SPIO and citrated mouse plasma as described previously.[2,49] High molecular weight kininogen cleavage fragments were visualized with Western blotting using rabbit anti-mouse antibody provided by the laboratory of Dr. Keith McCrae, Lerner Research Institute (Cleveland, OH).

Binding of Nanoparticles to SR-AI Immobilized on Beads. Five micrograms (at 0.2 mg/mL) of purified recombinant mouse SR-AI consisting of the extracellular domains fused to an N-terminal His_9 tag (R&D Systems; 1797-MS-050) was mixed with 50 μL of Ni-NTA Superflow beads (Qiagen, Valencia, CA) for 10 min at 4 °C. The beads were washed three times in PBS and mixed with SPIO (10 μL beads, 10 μg iron) or with liposomes (10 μL beads, 10 nmol lipid) at room temperature for 30 min. The beads were washed in 0.1% Tween-20/PBS three times.

The bound iron was visualized with Prussian blue stain and quantified with QuantiChrom iron assay, and the liposomes were visualized with a fluorescent microscope.

Computer Modeling of Receptor−SPIO Interaction. SR-AI forms a variety of conformations at physiological pH;[63] we build a nonfolded conformation for SR-AI model as described.[25] Dextran molecules were modeled using program InsightII (Accelrys, San Diego, CA). They were then minimized by 10 009 iterations steepest descent algorithm. Electrostatic interaction between full-length SR-AI and a plane of a crystal with the overall charge $4e^-$ has been calculated with the "Docking" module of the InsightII program with the dielectric constant 2. Crystallographic data of magnetite crystal[64] are available from variety of public databases (*e.g.*, http://www.crystallography.net). The 3D image of the magnetite crystal unit cell (rendered by jPOWD applet, Materials Data, Inc.) is available online (http://www.webmineral.com/jpowd/JPX/jpowd.php?target_file=Magnetite_33.jpx). The unit cell was rendered as a space-filled model with 100% atom volume, scaled 1:1 (using oxygen as a reference), and aligned with the extracellular part of SR-AI (collagen-like and cysteine-rich domains only) using image processing software (Adobe Photoshop CS3).

Conflict of Interest: The authors declare no competing financial interest.

Acknowledgment. We would like to thank Dr. Robert Mattrey (UCSD Department of Medicine) for providing us with Feridex I.V., and Dr. Ji-Ho Park (KAIST, Daejeon, South Korea) for helping us with the synthesis of SPIO and CLIO. We wish to thank Dr. Erkki Ruoslahti for discussions and comments during the work. This work was funded by 1R21CA137721-01 and 1R21CA167524-01 to D.S., and by the UCSD Cancer Center Specialized Support Grant P30 CA23100.

Supporting Information Available: Nanoparticle characterization data, high-resolution images of cells. This material is available free of charge *via* the Internet at http://pubs.acs.org.

REFERENCES AND NOTES

1. Lynch, I.; Salvati, A.; Dawson, K. A. Protein−Nanoparticle Interactions: What Does the Cell See? *Nat. Nanotechnol.* **2009**, *4*, 546–547.
2. Karmali, P. P.; Chao, Y.; Park, J. H.; Sailor, M. J.; Ruoslahti, E.; Esener, S. C.; Simberg, D. Different Effect of Hydrogelation on Antifouling and Circulation Properties of Dextran-Iron Oxide Nanoparticles. *Mol. Pharmaceutics* **2012**, *9*, 539–545.
3. Dobrovolskaia, M. A.; McNeil, S. E. Immunological Properties of Engineered Nanomaterials. *Nat. Nanotechnol.* **2007**, *2*, 469–478.
4. Moghimi, S. M.; Hunter, A. C.; Murray, J. C. Long-Circulating and Target-Specific Nanoparticles: Theory to Practice. *Pharmacol. Rev.* **2001**, *53*, 283–318.
5. Kamps, J. A.; Scherphof, G. L. Receptor *versus* Non-receptor Mediated Clearance of Liposomes. *Adv. Drug Delivery Rev.* **1998**, *32*, 81–97.
6. Andersen, A. J.; Hashemi, S. H.; Andresen, T. L.; Hunter, A. C.; Moghimi, S. M. Complement: Alive and Kicking Nanomedicines. *J. Biomed. Nanotechnol.* **2009**, *5*, 364–372.
7. Karmali, P. P.; Simberg, D. Interactions of Nanoparticles with Plasma Proteins: Implication on Clearance and Toxicity of Drug Delivery Systems. *Expert Opin. Drug Delivery* **2011**, *8*, 343–357.
8. Miyanishi, M.; Tada, K.; Koike, M.; Uchiyama, Y.; Kitamura, T.; Nagata, S. Identification of Tim4 as a Phosphatidylserine Receptor. *Nature* **2007**, *450*, 435–439.
9. Shimaoka, T.; Kume, N.; Minami, M.; Hayashida, K.; Kataoka, H.; Kita, T.; Yonehara, S. Molecular Cloning of a Novel Scavenger Receptor for Oxidized Low Density Lipoprotein, Sr-Psox, on Macrophages. *J. Biol. Chem.* **2000**, *275*, 40663–40666.
10. Krieger, M.; Herz, J. Structures and Functions of Multiligand Lipoprotein Receptors—Macrophage Scavenger Receptors and Ldl Receptor-Related Protein (Lrp). *Annu. Rev. Biochem.* **1994**, *63*, 601–637.
11. Shnyra, A.; Lindberg, A. A. Scavenger Receptor Pathway for Lipopolysaccharide Binding to Kupffer and Endothelial Liver Cells *in Vitro*. *Infect. Immun.* **1995**, *63*, 865–873.
12. Xu, Z. L.; Tian, J.; Smith, J. S.; Byrnes, A. P. Clearance of Adenovirus by Kupffer Cells Is Mediated by Scavenger Receptors, Natural Antibodies, and Complement. *J. Virol.* **2008**, *82*, 11705–11713.
13. Kanno, S.; Furuyama, A.; Hirano, S. A Murine Scavenger Receptor Marco Recognizes Polystyrene Nanoparticles. *Toxicol. Sci.* **2007**, *97*, 398–406.
14. Nagayama, S.; Ogawara, K.; Minato, K.; Fukuoka, Y.; Takakura, Y.; Hashida, M.; Higaki, K.; Kimura, T. Fetuin Mediates Hepatic Uptake of Negatively Charged Nanoparticles *via* Scavenger Receptor. *Int. J. Pharm.* **2007**, *329*, 192–198.
15. Zhang, L. W.; Monteiro-Riviere, N. A. Mechanisms of Quantum Dot Nanoparticle Cellular Uptake. *Toxicol. Sci.* **2009**, *110*, 138–155.
16. Kobzik, L. Lung Macrophage Uptake of Unopsonized Environmental Particulates. Role of Scavenger-Type Receptors. *J. Immunol.* **1995**, *155*, 367–376.
17. Patel, P. C.; Giljohann, D. A.; Daniel, W. L.; Zheng, D.; Prigodich, A. E.; Mirkin, C. A. Scavenger Receptors Mediate Cellular Uptake of Polyvalent Oligonucleotide-Functionalized Gold Nanoparticles. *Bioconjugate Chem.* **2010**, *21*, 2250–2256.
18. Nahrendorf, M.; Keliher, E.; Marinelli, B.; Waterman, P.; Feruglio, P. F.; Fexon, L.; Pivovarov, M.; Swirski, F. K.; Pittet, M. J.; Vinegoni, C.; *et al.* Hybrid Pet-Optical Imaging Using Targeted Probes. *Proc. Natl. Acad. Sci. U.S.A.* **2010**, *107*, 7910–7915.
19. Gazeau, F.; Levy, M.; Wilhelm, C. Optimizing Magnetic Nanoparticle Design for Nanothermotherapy. *Nanomedicine* **2008**, *3*, 831–844.
20. Figuerola, A.; Di Corato, R.; Manna, L.; Pellegrino, T. From Iron Oxide Nanoparticles towards Advanced Iron-Based Inorganic Materials Designed for Biomedical Applications. *Pharmacol. Res.* **2010**, *62*, 126–143.
21. Gupta, A. K.; Gupta, M. Synthesis and Surface Engineering of Iron Oxide Nanoparticles for Biomedical Applications. *Biomaterials* **2005**, *26*, 3995–4021.
22. Lunov, O.; Zablotskii, V.; Syrovets, T.; Rocker, C.; Tron, K.; Nienhaus, G. U.; Simmet, T. Modeling Receptor-Mediated Endocytosis of Polymer-Functionalized Iron Oxide Nanoparticles by Human Macrophages. *Biomaterials* **2011**, *32*, 547–555.
23. Raynal, I.; Prigent, P.; Peyramaure, S.; Najid, A.; Rebuzzi, C.; Corot, C. Macrophage Endocytosis of Superparamagnetic Iron Oxide Nanoparticles: Mechanisms and Comparison of Ferumoxides and Ferumoxtran-10. *Invest. Radiol.* **2004**, *39*, 56–63.
24. Chao, Y.; Karmali, P. P.; Simberg, D. Role of Carbohydrate Receptors in the Macrophage Uptake of Dextran-Coated Iron Oxide Nanoparticles. *Adv. Exp. Med. Biol.* **2012**, *733*, 115–123.
25. Chao, Y.; Makale, M.; Karmali, P. P.; Sharikov, Y.; Tsigelny, I.; Merkulov, S.; Kesari, S.; Wrasidlo, W.; Ruoslahti, E.; Simberg, D. Recognition of Dextran-Superparamagnetic Iron Oxide Nanoparticle Conjugates (Feridex) *via* Macrophage Scavenger Receptor Charged Domains. *Bioconjugate Chem.* **2012**, *23*, 1003–1009.
26. Boehm, H. P. Acidic and Basic Properties of Hydroxylated Metal-Oxide Surfaces. *Discuss. Faraday Soc.* **1971**, 264–267.
27. Bautista, M. C.; Bomati-Miguel, O.; Morales, M. D.; Serna, C. J.; Veintemillas-Verdaguer, S. Surface Characterisation of Dextran-Coated Iron Oxide Nanoparticles Prepared by Laser Pyrolysis and Coprecipitation. *J. Magn. Magn. Mater.* **2005**, *293*, 20–27.
28. Jung, C. W. Surface Properties of Superparamagnetic Iron Oxide MR Contrast Agents: Ferumoxides, Ferumoxtran, Ferumoxsil. *Magn. Reson. Imaging* **1995**, *13*, 675–691.
29. Lucas, I. T.; Durand-Vidal, S.; Dubois, E.; Chevalet, J.; Turq, P. Surface Charge Density of Maghemite Nanoparticles: Role of Electrostatics in the Proton Exchange. *J. Phys. Chem. C* **2007**, *111*, 18568–18576.

30. Doi, T.; Higashino, K.; Kurihara, Y.; Wada, Y.; Miyazaki, T.; Nakamura, H.; Uesugi, S.; Imanishi, T.; Kawabe, Y.; Itakura, H.; *et al.* Charged Collagen Structure Mediates the Recognition of Negatively Charged Macromolecules by Macrophage Scavenger Receptors. *J. Biol. Chem.* **1993**, *268*, 2126–2133.
31. Pearson, A. M.; Rich, A.; Krieger, M. Polynucleotide Binding to Macrophage Scavenger Receptors Depends on the Formation of Base-Quartet-Stabilized Four-Stranded Helices. *J. Biol. Chem.* **1993**, *268*, 3546–3554.
32. Krieger, M.; Herz, J. Structures and Functions of Multiligand Lipoprotein Receptors: Macrophage Scavenger Receptors and Ldl Receptor-Related Protein (Lrp). *Annu. Rev. Biochem.* **1994**, *63*, 601–637.
33. Perrault, S. D.; Walkey, C.; Jennings, T.; Fischer, H. C.; Chan, W. C. Mediating Tumor Targeting Efficiency of Nanoparticles through Design. *Nano Lett.* **2009**, *9*, 1909–1915.
34. Alexis, F.; Pridgen, E.; Molnar, L. K.; Farokhzad, O. C. Factors Affecting the Clearance and Biodistribution of Polymeric Nanoparticles. *Mol. Pharmaceutics* **2008**, *5*, 505–515.
35. Win, K. Y.; Feng, S. S. Effects of Particle Size and Surface Coating on Cellular Uptake of Polymeric Nanoparticles for Oral Delivery of Anticancer Drugs. *Biomaterials* **2005**, *26*, 2713–2722.
36. Petros, R. A.; DeSimone, J. M. Strategies in the Design of Nanoparticles for Therapeutic Applications. *Nat. Rev. Drug Discovery* **2010**, *9*, 615–627.
37. Li, S. D.; Huang, L. Pharmacokinetics and Biodistribution of Nanoparticles. *Mol. Pharmaceutics* **2008**, *5*, 496–504.
38. Wu, Y. J.; Muldoon, L. L.; Varallyay, C.; Markwardt, S.; Jones, R. E.; Neuwelt, E. A. *In Vivo* Leukocyte Labeling with Intravenous Ferumoxides/Protamine Sulfate Complex and *In Vitro* Characterization for Cellular Magnetic Resonance Imaging. *Am. J. Physiol.* **2007**, *293*, C1698–C1708.
39. Plourde, N. M.; Kortagere, S.; Welsh, W.; Moghe, P. V. Structure−Activity Relations of Nanolipoblockers with the Atherogenic Domain of Human Macrophage Scavenger Receptor A. *Biomacromolecules* **2009**, *10*, 1381–1391.
40. Daldrup-Link, H. E.; Golovko, D.; Ruffell, B.; Denardo, D. G.; Castaneda, R.; Ansari, C.; Rao, J.; Tikhomirov, G. A.; Wendland, M. F.; Corot, C.; *et al.* MRI of Tumor-Associated Macrophages with Clinically Applicable Iron Oxide Nanoparticles. *Clin. Cancer Res.* **2011**, *17*, 5695–5704.
41. Chen, W. C.; Kawasaki, N.; Nycholat, C. M.; Han, S.; Pilotte, J.; Crocker, P. R.; Paulson, J. C. Antigen Delivery to Macrophages Using Liposomal Nanoparticles Targeting Sialoadhesin/Cd169. *PLoS One* **2012**, *7*, e39039.
42. Denizli, B. K.; Can, H. K.; Rzaev, Z. M. O.; Guner, A. Preparation Conditions and Swelling Equilibria of Dextran Hydrogels Prepared by Some Crosslinking Agents. *Polymer* **2004**, *45*, 6431–6435.
43. Park, J. H.; von Maltzahn, G.; Zhang, L.; Derfus, A. M.; Simberg, D.; Harris, T. J.; Ruoslahti, E.; Bhatia, S. N.; Sailor, M. J. Systematic Surface Engineering of Magnetic Nanoworms for *In Vivo* Tumor Targeting. *Small* **2009**, *5*, 694–700.
44. Jung, C. W.; Jacobs, P. Physical and Chemical Properties of Superparamagnetic Iron Oxide MR Contrast Agents: Ferumoxides, Ferumoxtran, Ferumoxsil. *Magn. Reson. Imaging* **1995**, *13*, 661–674.
45. Sugiura, M.; Ito, A.; Ogiso, T.; Kato, K.; Asano, H. Studies on Dextranase. Purification of Dextranase from Penicillium Funiculosum and Its Enzymatic Properties. *Biochim. Biophys. Acta* **1973**, *309*, 357–362.
46. Doshi, N.; Mitragotri, S. Macrophages Recognize Size and Shape of Their Targets. *PLoS One* **2010**, *5*, e10051.
47. Champion, J. A.; Mitragotri, S. Role of Target Geometry in Phagocytosis. *Proc. Natl. Acad. Sci. U.S.A.* **2006**, *103*, 4930–4934.
48. Arnida; Janat-Amsbury, M. M.; Ray, A.; Peterson, C. M.; Ghandehari, H. Geometry and Surface Characteristics of Gold Nanoparticles Influence Their Biodistribution and Uptake by Macrophages. *Eur. J. Pharm. Biopharm.* **2011**, *77*, 417–423.
49. Simberg, D.; Zhang, W. M.; Merkulov, S.; McCrae, K.; Park, J. H.; Sailor, M. J.; Ruoslahti, E. Contact Activation of Kallikrein−Kinin System by Superparamagnetic Iron Oxide Nanoparticles *in Vitro* and *in Vivo*. *J. Controlled Release* **2009**, *140*, 301–305.
50. Petrache, H. I.; Tristram-Nagle, S.; Gawrisch, K.; Harries, D.; Parsegian, V. A.; Nagle, J. F. Structure and Fluctuations of Charged Phosphatidylserine Bilayers in the Absence of Salt. *Biophys. J.* **2004**, *86*, 1574–1586.
51. Jolstera, R.; Gunneriusson, L.; Holmgren, A. Surface Complexation Modeling of Fe_3O_4−H+ and Magnesium(II) Sorption onto Maghemite and Magnetite. *J. Colloid Interface Sci.* **2012**, *386*, 260–267.
52. Ohsawa, K.; Murata, M.; Ohshima, H. Zeta-Potential and Surface-Charge Density of Polystyrene-Latex—Comparison with Synaptic Vesicle and Brush-Border Membrane Vesicle. *Colloid Polym. Sci.* **1986**, *264*, 1005–1009.
53. Kawaguchi, T.; Hasegawa, M. Structure of Dextran-Magnetite Complex: Relation between Conformation of Dextran Chains Covering Core and Its Molecular Weight. *J. Mater. Sci.* **2000**, *11*, 31–35.
54. Gessner, A.; Lieske, A.; Paulke, B.; Muller, R. Influence of Surface Charge Density on Protein Adsorption on Polymeric Nanoparticles: Analysis by Two-Dimensional Electrophoresis. *Eur. J. Pharm. Biopharm.* **2002**, *54*, 165–170.
55. Dos Santos, N.; Allen, C.; Doppen, A. M.; Anantha, M.; Cox, K. A.; Gallagher, R. C.; Karlsson, G.; Edwards, K.; Kenner, G.; Samuels, L.; *et al.* Influence of Poly(ethylene glycol) Grafting Density and Polymer Length on Liposomes: Relating Plasma Circulation Lifetimes to Protein Binding. *Biochim. Biophys. Acta* **2007**, *1768*, 1367–1377.
56. Yamamoto, K.; Nishimura, N.; Doi, T.; Imanishi, T.; Kodama, T.; Suzuki, K.; Tanaka, T. The Lysine Cluster in the Collagen-like Domain of the Scavenger Receptor Provides for Its Ligand Binding and Ligand Specificity. *FEBS Lett.* **1997**, *414*, 182–186.
57. Neyen, C.; Pluddemann, A.; Roversi, P.; Thomas, B.; Cai, L.; van der Westhuyzen, D. R.; Sim, R. B.; Gordon, S. Macrophage Scavenger Receptor a Mediates Adhesion to Apolipoproteins a-I and E. *Biochemistry* **2009**, *48*, 11858–11871.
58. Goss, C. J. Saturation Magnetization, Coercivity and Lattice-Parameter Changes in the System Fe_3O_4-γ-Fe_2O_3, and Their Relationship to Structure. *Phys. Chem. Miner.* **1988**, *16*, 164–171.
59. Simberg, D.; Park, J. H.; Karmali, P. P.; Zhang, W. M.; Merkulov, S.; McCrae, K.; Bhatia, S. N.; Sailor, M.; Ruoslahti, E. Differential Proteomics Analysis of the Surface Heterogeneity of Dextran Iron Oxide Nanoparticles and the Implications for Their *In Vivo* Clearance. *Biomaterials* **2009**, *30*, 3926–3933.
60. Kansal, S.; Tandon, R.; Dwivedi, P.; Misra, P.; Verma, P. R.; Dube, A.; Mishra, P. R. Development of Nanocapsules Bearing Doxorubicin for Macrophage Targeting through the Phosphatidylserine Ligand: A System for Intervention in Visceral Leishmaniasis. *J. Antimicrob. Chemother.* **2012**, *67*, 2650–2660.
61. Park, J. H.; von Maltzahn, G.; Zhang, L.; Schwartz, M. P.; Ruoslahti, E.; Bhatia, S.; Sailor, M. J. Magnetic Iron Oxide Nanoworms for Tumor Targeting and Imaging. *Adv. Mater.* **2008**, *20*, 1630–1635.
62. Litovsky, S.; Madjid, M.; Zarrabi, A.; Casscells, S. W.; Willerson, J. T.; Naghavi, M. Superparamagnetic Iron Oxide-Based Method for Quantifying Recruitment of Monocytes to Mouse Atherosclerotic Lesions *in Vivo*: Enhancement by Tissue Necrosis Factor-alpha, Interleukin-1beta, and Interferon-gamma. *Circulation* **2003**, *107*, 1545–1549.
63. Resnick, D.; Chatterton, J. E.; Schwartz, K.; Slayter, H.; Krieger, M. Structures of Class a Macrophage Scavenger Receptors. Electron Microscopic Study of Flexible, Multidomain, Fibrous Proteins and Determination of the Disulfide Bond Pattern of the Scavenger Receptor Cysteine-Rich Domain. *J. Biol. Chem.* **1996**, *271*, 26924–26930.
64. Oneill, H. S.; Dollase, W. A. Crystal-Structures and Cation Distributions in Simple Spinels from Powder XRD Structural Refinements—$MgCr_2O_4$, $ZnCr_2O_4$, Fe_3O_4 and the Temperature-Dependence of the Cation Distribution in $ZnAl_2O_4$. *Phys. Chem. Miner.* **1994**, *20*, 541–555.